RSC Advances

PAPER

View Article Online
View Journal | View Issue

Cite this: *RSC Adv.*, 2020, **10**, 5399

Experimental and DFT studies on the ultrasonic energy-assisted extraction of the phytochemicals of *Catharanthus roseus* as green corrosion inhibitors for mild steel in NaCl medium†

N. Palaniappan, *[a] I. Cole, *[b] F. Caballero-Briones, [c] S. Manickam, [d] K. R. Justin Thomas [e] and D. Santos [f]

Received 31st October 2019
Accepted 10th December 2019

DOI: 10.1039/c9ra08971c

rsc.li/rsc-advances

Catharanthus roseus (Apocynaceae family) extract is rich in organic phytochemicals such as alkaloids, polyphenolic compounds, and flavonoids. It contains several functional entities such as fused heterocycles, and hydroxyl and carbonyl groups, which could be useful for corrosion inhibition of mild steel in NaCl environments. In the present work, ultrasonic energy was used to obtain the ethanolic extracts of root and stem which were then tested as corrosion inhibitors for mild steel in the presence of 3.5% NaCl. The corrosion inhibition process was studied by UV-visible spectroscopy, Fourier transform infrared spectroscopy, atomic force microscopy, weight loss, and electrochemical methods. After immersing in the corrosive medium, the microstructures of mild steel were investigated by scanning electron microscopy, X-ray diffraction, and ellipsometry. The extract of *C. roseus* showed excellent adsorption on mild steel surface as confirmed by DFT calculations. The results indicate that the extract of *C. roseus* acts as a mixed type corrosion inhibitor, where the stem extract is the most efficient inhibitor in 3.5% NaCl solution possibly due to the higher active area of stem phytochemicals.

1. Introduction

The oil, gas, and construction industries are major users of mild steel and face severe corrosion problems due to the presence of a frail barrier layer.[1] Traditionally, organic inhibitors are used to protect structures from corrosive attack, but unfortunately such organic inhibitors often contain chemicals that are toxic both to humans and aquatic life. Therefore, there is a need for eco-friendly inhibitors in preventing corrosion.[2] Recently, extracts obtained from medicinal plants have been developed as green corrosion inhibitors for mild steel and their alloys.[3,4] Many of the phytochemical constituents in the extracts obtained from leaves, stem and roots of plants have been found to possess strong anti-corrosion properties. Early work reported that alkaloids isolated from the extracts of date palm seed effectively reduced acid corrosion in carbon steel.[5] *Catharanthus roseus* is an ancient herbal medicinal plant useful for different ailments such as cancer, diabetes, and leukemia. This plant presents different phenolic compounds that have shown antioxidant activity.[6] On the other hand, Strube *et al.* investigated the extraction of polyphenols from black tea using conventional and ultrasonic methods and found that the yield from ultrasonic-assisted extraction was higher than the conventional methods.[7] Li *et al.* conducted extraction of alkaloids from the medicinal plant *Phellodendron amurense* Rupr. using ionic liquids as solvent and by using ultrasonic energy and noted that the extraction yield was around 99.99% and a higher yield was proposed due to intense bubble collapse from ultrasound energy which assisted diffusion to plant matrix.[8] Rai *et al.* investigated ultrasonic energy assisted alkaloids extraction from potato peel. The extracted yields were more than 90% owing to ultrasound which uniformly distributed the energy to the potato peel matrix and without causing any damage to the structure of alkaloids.[9] Also, phytochemicals obtained using conventional method were used as corrosion inhibitors under different conditions. Oguzie *et al.* studied the extraction of phytochemicals from *Piper guineense* using acid as a solvent at 70 °C. Whereas, the bio active alkaloids derivatives may be affected due to the inorganic acidic and high temperature.[10]

[a]*School Chemicals Sciences, Central University of Gujarat, India. E-mail: palaniappancecri@rediffmail.com*

[b]*ECP Director, Adv. Manufacture and Fabrication, RMIT University, Australia. E-mail: ivan.cole@rmit.edu.au*

[c]*Instituto Politecnico, Nacional, Materials, and Technologies for Energy, Health, and Environment (GESMAT), CICATA Altamira, 89600, Altamira, Mexico*

[d]*Faculty of Science and Engineering, University of Nottingham Malaysia, Jalan Broga, Semenyih, Kuala Lumpur 43500, Malaysia*

[e]*Organic Materials Laboratory, Department of Chemistry, Indian Institute of Technology Roorkee, Roorkee 247667, India*

[f]*Computing Institute, Federal University of Alagoas, 57038-00, Brazil*

† Electronic supplementary information (ESI) available. See DOI: 10.1039/c9ra08971c

Oguzie *et al.* conducted the extraction of *Capsicum frutescens* refluxing with ethanol. The key problem with polar medium is that non-polar phytochemicals are not extracted, which may affect the efficiency of corrosion inhibition, as non-polar alkaloids exhibit strong physisorption as compared with polar phytochemicals.[11] Oguzie *et al.* also reported on ethanol based extraction of *Kola nitida* medicinal plant, and the extract of which was used as a green corrosion inhibitor due to the presence of active polyphenols that adsorb on the steel surface.[12] *Opuntia elatior* and *Anthemis pseudocotula* have also been extracted using alcoholic solution and were investigated for their corrosion inhibition on mild steel in acid medium, where the complex chemical structure of phytochemicals chemisorbed on the steel surface and reduced the corrosion rate.[13,14] Sahin *et al.* observed that acidic conditions extracted phytochemicals from *Schinopsis lorentzii* and which acted as corrosion inhibitor in an acidic medium.[15] The inhibition efficiency of phytochemicals extracted in acid media decreased due to the damage of the fused ring of flavonoid with acid environments. Umoren *et al.* reported date palm seed phytochemicals extracted in acid medium which demonstrated mixed-type inhibitor behaviour with inhibition efficiency around 80%.[16] Khadraoui investigated the extraction of *Thymus algeriensis* using strong inorganic acid medium, with a 75% corrosion inhibition attributed to the alkaloids in the extract. The extraction of *T. algeriensis* was studied for corrosion inhibition in an acidic medium on mild steel and the inhibition efficiency was found to be 76% due to the alkaloids affected by acid.[17] The medicinal plants of *Mensa alliacea* and *Rhus verniciflua* were also extracted using ethanol as solvent and the corrosion inhibition was studied on mild steel using 3.5% NaCl and 1 M sulphuric acid. The corrosion inhibition efficiency decreased as the non-polar phytochemicals were not extracted.[18,19] Phytochemicals from *Xylopiaa aethiopica*, *Moringa oleifera*, and *Urfrica dioia* were extracted by conventional soaking method and the corrosion inhibition efficiency were investigated in acidic and salt environments,[20–26] where the corrosion inhibition efficiency was decreased again as non-polar phytochemicals were not extracted by conventional methods. Based on the above studies, to overcome conventional extraction problems, in this investigation, polar and non-polar phytochemicals extraction was performed by ultrasonic energy. The 3.5% NaCl corrosion medium is chosen to mimic seawater salinity concentration.

2. Experimental section

2.1. Extraction

Catharanthus roseus (*C. roseus*) plants were collected from Nagarajan Kamalakanni farm field in Pulavarnatham, India. The collected plants were dried in sunlight for one week, the roots and stems were separated, and then grinded in powder form for extraction, 100 g powder of *C. roseus* stems or roots was added to 100 mL ethanol in two different round bottom flasks. Then, continuous sonication was carried out for 1 h at 80 kHz by using a SB-300 DTY Multi Ultrasonicator. After sonication, the undissolved material was removed from the mixture. Then, ethanol was vacuum evaporated to obtain 1 g of green solid product. Extracts obtained using both stem and roots were tested as corrosion inhibitors, without any further purification.

2.2. Materials

Mild steel (MS) coupons (C: 0.16, Mn: 0.032, Si: 0.08, S: 0.026, P: 0.03, and rest Fe, all in wt%) were polished with a series of silicon carbide papers from 600 to 1200 before the corrosion inhibition experiments. Each electrode was immersed for 5 days in 3.5% NaCl solution containing 5 mg mL^{-1} of the root or stem extracts of *C. roseus* as shown in Fig. 1.

2.3. Characterization of barrier layer

The film adhered on the surface of MS during the immersion in the NaCl solution with the stem or root extracts, was carefully removed with a spatula, dried and mixed with pure KBr, and pelletized for FTIR measurements. The functional groups were analysed by Fourier Transform Infrared Spectroscopy (PerkinElmer, Spectrum 65). The adsorbed biofilm was dispersed in deionized water and studied by UV-visible spectroscopy. The analysis was carried out in the range of 200–600 nm at room temperature using Spectro UV model 2060+. The topography of the mild steel surface was investigated by atomic force microscopy before and after continuous immersion in 3.5 wt% NaCl medium for five days with and without inhibitor. The thickness of the protective layer formed onto the mild steel was measured by Ellipsometer in a Horiba-UVISEL from 1.5 to 6 eV using incident light at 70°. The roughness analysis of the of mild steel surface was carried out using an NT-MDF atomic force microscope in the contact mode using Si tips with a spring constant of 4 N m^{-1}. After exposition to the corrosive media, the products onto the MS coupons were studied by X-ray diffraction in a D8 Advance diffractometer from Bruker, using Cu Kα radiation (0.15418 nm). Raman spectra were acquired in a Raman WITec instrument using a 532 nm laser. The functional groups of the *C. roseus* extracts adsorbed on the mild steel coupons were studied by AT-FTIR (Thermo Fisher iD7 Nicole iS5 Spectrometer).

2.4. Weight loss measurements

The MS coupons (3 length $\times$ 1 width cm^2) were first weighed in a balance (Kern ABS) with a sensitivity of $\pm$ 0.0001 g before and after immersion in 5 mg of extraction 100 mL solution of NaCl (3.5 wt%) for five days. The system was maintained at 35 $\pm$ 1 °C.

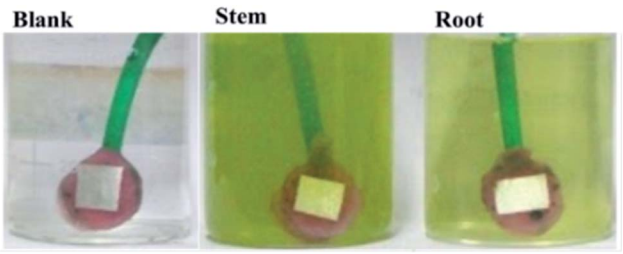

Fig. 1 Mild steel coupons 5 days immersed in 3.5 wt% NaCl in the different *C. roseus* extracts, blank (left), stem, (middle) and root, (right).

The inhibition efficiency (η) and surface coverage (θ) were calculated with eqn (1) and (2) as follows

$$\eta = \frac{w_0 - w_i}{w_0} \times 100 \quad (1)$$

$$\theta = \frac{w_0 - w_i}{w_0} \quad (2)$$

where w_0 and w_i are respectively the weight loss (g) of mild steel in the absence and presence of inhibitor. The corrosion rates (Cr) of MS in the presence of the different extracts of *C. roseus* were calculated by the following eqn (3).

$$\text{mmpy} = \frac{87.6w}{Atd} \quad (3)$$

where mmpy represents millimetres per year, w indicates the weight loss (milligrams), A represents the area of the specimen (cm^2) exposed in a medium of NaCl, t represents the immersion time (h) and d indicates the density of mild steel (g cm^2).

2.5. Electrochemical studies

The electrochemical studies were carried out at room temperature in a three-electrode configuration, using a CHI920D electrochemical station. The mild steel coupons were used as the working electrode, Ag/AgCl (KCl sat) as the reference electrode, and a large-area platinum mesh as the counter electrode. The open circuit potential (OCP) was measured before starting the electrochemical test. For the Tafel plots, the potential was scanned over a range of ±250 mV with respect to OCP at a sweep rate of 0.5 mV s^{-1}. The linear segments of the anodic and cathodic polarization curves were extrapolated to obtain the corrosion current densities (I_{corr}) and corrosion potentials (E_{corr}) by using CHI 920D software. Then, the corrosion inhibition efficiency was calculated by the eqn (4) and (5).

$$\eta = \frac{I_0 - I_i}{I_0} \times 100 \quad (4)$$

where I_0 and I_i are the corrosion current densities with and without inhibitor, respectively. Electrochemical impedance spectroscopy (EIS) was done from 0.01 MHz to 100 kHz at open circuit potential using excitation amplitude of 10 mV. From the EIS data, the capacitance of the adhered film was calculated assuming a RRC circuit, and standard deviation using eqn (5) and (6).

$$C_{dl} = \frac{1}{2\pi \max f R_{ct}} \quad (5)$$

$$S = \frac{\sqrt{\sum X - X^-}}{N - 1} \quad (6)$$

where C_{dl} double layer capacitor, s = standard deviation, X samples, X^- variance.

2.6. Theoretical studies

All the calculations were carried out using Gaussian 09 suite program. The geometrical optimizations were performed at B3LYP/6-31G* level of theory. On each geometry, the frequency calculations were attempted at the same level of theory to check the minima (zero negative frequency). The effects of ethanol (as a solvent during the reaction) were incorporated using polarizable continuum model (PCM) at B3LYP/TZVP level of theory. Theoretical parameters such as the highest occupied molecular orbital (HOMO), the lowest unoccupied molecular orbital (LUMO), and the energy gap between E_{LUMO} and E_{HOMO} ($\Delta E = E_{LUMO} - E_{HOMO}$) were obtained. The electronegativity (χ) associated with corrosion inhibition efficiency and chemical hardness (η), softness (σ), electrophilicity (ω), and ΔN were calculated using the eqn (6)–(10).

$$\chi = \frac{I + A}{2} \quad (7)$$

$$\eta = \frac{I - A}{2} \quad (8)$$

$$\sigma = \frac{1}{\eta} \quad (9)$$

$$\omega = \frac{\chi^2}{2\eta} \quad (10)$$

$$\Delta E = \frac{\chi_{Fe} - Fe_{inh}}{2\eta_{Fe} - \eta_{inh}} \quad (11)$$

3. Results and discussion

3.1. Spectroscopic characterization

FTIR were carried out in the fresh extracts as well as in the adsorbed film formed upon immersion of MS into the 3.5%

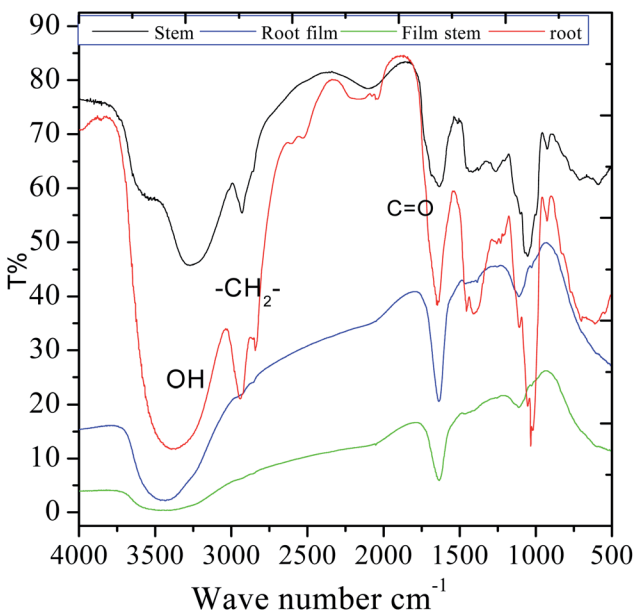

Fig. 2 FTIR spectra of the *C. roseus* extracts and of the film formed onto mild steel during the immersion in the 3.5% NaCl medium + stem or root extracts.

NaCl solution with the *C. roseus* extracts. As shown in Fig. 2, the spectrum of the stem extract presents a broad peak at 3500 cm^{-1} which is associated with polyphenolic compounds. Further, the sharp peak appearing at 2927 cm^{-1} is associated with the stretching of alkyl C–H. The peak at 1680 cm^{-1} can be associated with C=O stretching, and also to the stretching of a quinonoid form. A strong band appearing at 1460 cm^{-1} corresponds to C–H bond bending. The peak at 980 cm^{-1} corresponds to the stretching vibrations of epoxy groups and a small peak at 924 cm^{-1} is ascribed to $-CH=CH_2$ bond vibration; the broad peak at 520 cm^{-1} is related to the vibrations of C–H bond in aromatic systems. The HRSM spectra of the phytochemicals of *C. roseus* extract are shown in Fig. S1 and S2 (ESI†) and it could be found that resemble to authentic result. The mass results suggested that the phytochemical flavonoid from *C. roseus* extracted was 95%. In the case of phytochemicals extracted from the root, the broad band at 3388 cm^{-1} can be ascribed to OH stretching. After 5 days of immersing mild steel in the corrosion medium, the films formed onto the coupons were studied by FTIR after being removed and put into KBr pellets. The shifting of the stretching frequency of functional groups of *C. roseus* indicating that the nonbonding electrons of *C. roseus* interact with the surface of mild steel. The stretching of hydroxyl bond at 3400 cm^{-1} became narrow possibly due to the interaction of hydroxyl groups with the metal surface. However, the stretching of carbonyl and other groups were changed due to the interaction of free electrons with the mild steel surface.

Fig. 3 shows the UV-visible absorption before and after immersion of mild steel in the extract of *C. roseus* containing 3.5% NaCl solution. Before immersion, absorption spectra of stem and root extracts is dominated by peaks at 380, and 350 nm arising from the π–π* absorption of flavonoid active species. However, after immersion, the absorption wavelength of stem and root extracts decreased from 350 to 330 nm, which could be due to the chemisorption of bisindole on polarised mild steel surface.[27–30] The strong absorption band of stem extract appearing at 380 nm is associated with the electronic transition between the π–π* and n–π* energy levels. However, the absorption bands from each extract are noticeably different from purely extracted phytochemicals due to the interaction of polyphenolic compounds on the mild steel surface.[28–32] The UV-vis absorption spectroscopy supports the adsorption of extract molecules on the mild steel surface.

As shown in Fig. 4, after corrosion treatment, the film thickness of self-assembled layer deposited on mild steel with and without (blank) inhibitor molecules was investigated using incident light at 70°. The blank mild steel surfaces indicates that there is no film on the mild steel surface due to the absence of inhibitor molecules, and only iron oxide layer is formed on the mild steel surface. Further, the film thickness of blank mild steel oxide layer is 3.1159 Å, and the film thickness is less as compared to the presence of inhibitor owing to the corrosion product on the steel surface. Also, the model fitting values were increased (χ^2, 86.8779), indicating that there is no uniform oxide layer on the steel surface.

On the another hand, the presence of inhibitor molecules (root and stem extracts) from the experimental blue lines are fitted with the model and it has been found that the inhibitor molecules are uniformly adsorbed on the steel surface. Further, the film thickness values of root (962.5060 Å) and stem (1694.9741 Å) were increased due to the chemisorption of inhibitor molecules on mild steel.[33–36] The obtained film thickness values are presented in Table 1. The results of Ellipsometer studies revealed that there is excellent chemisorption of *C. roseus* on the mild steel surface.

3.2. Surface wettability

After 5 days of immersing mild steel in 3.5% NaCl with and without inhibitor molecules the surface wettability was studied and the results are shown in Fig. 5. The blank mild steel surface presents high hydrophobicity due to the iron oxides (Fe_2O_3) on the surface.[37–39]

However, the surface wettability of mild steel immersed in the phytochemicals of root and stem extracts showed a value

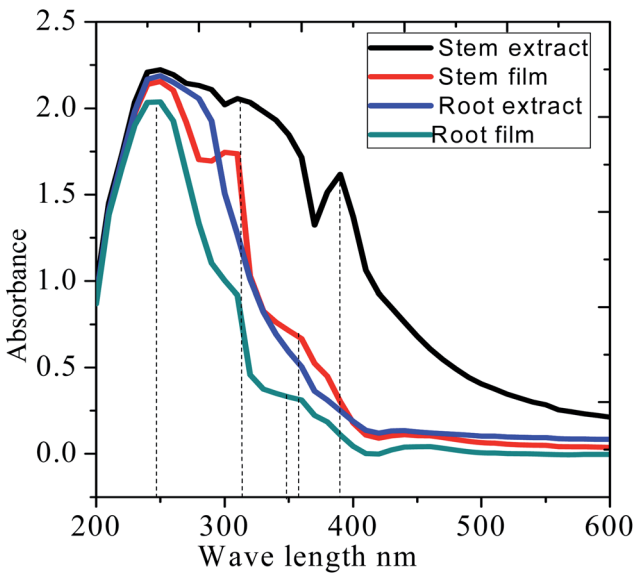

Fig. 3 UV-absorption spectra of the *C. roseus* extracts before and after mild steel immersion in 3.5% NaCl.

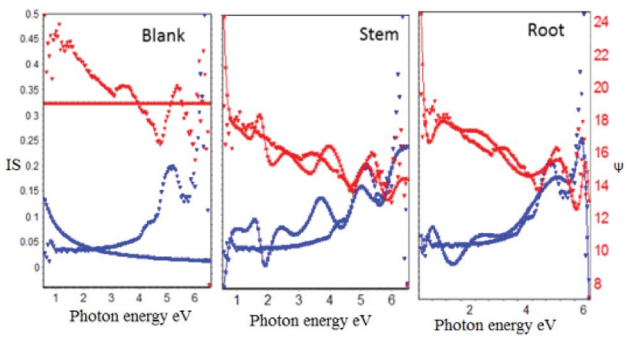

Fig. 4 Film thickness of inhibitor molecules adsorbed on mild steel surface.

Table 1 Corrosion data of mild steel immersed 5 days in 3.5% NaCl medium with and without inhibitor molecules

S. no.	Weight loss (g cm^{-1})	Surface coverage (θ)	Cr (mmpy)	IE (%)	Model fitting (χ^2)	Thickness (Å)
Blank	0.0758	—	0.1173	—	86.8779	3.1159
Root	0.0117	0.8448	0.0182	84	1.2147	1694.9741
Stem	0.0028	0.9630	0.0043	96	1.8044	962.5060

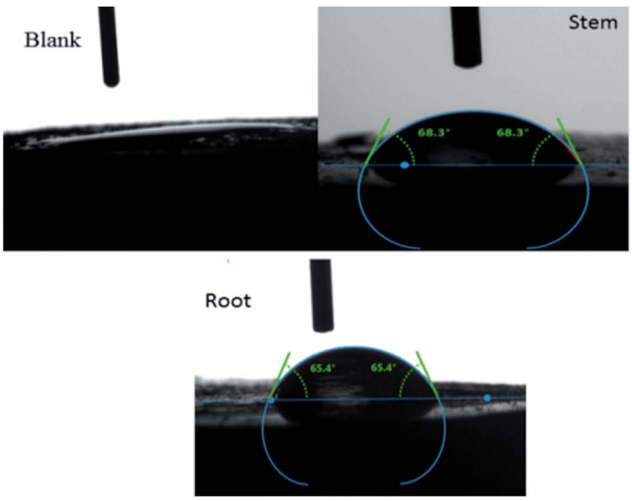

Fig. 5 The surface wettability of mild steel immersed with and without inhibitor.

around.[67,68] due to the presence of an organic film on the steel surface.

3.3. AFM surface analysis

Fig. 6 shows the AFM images of mild steel exposed in the presence and absence of extract under 3.5% NaCl solution. The polished mild steel shows a featureless and smooth surface. In the case of mild steel coupon immersed in 3.5% NaCl solution without any inhibitor, the surface roughness increased indicating that the mild steel undergoes corrosion.

The mild steel surface has pit corrosion due to the physisorbed chloride ions on the mild steel. In the case of mild steel immersed in the phytochemicals of stem, the surface is corrugated possibly because the phytochemicals are agglomerated on the steel surface however there is no evidence of surface attack, or pits.[40,41]

The microstructure of mild steel immersed in the phytochemicals of root extract demonstrates a smooth surface with some evidence of crevices due to the initiation of localized corrosion on the mild steel surface. Earlier results reported that the extracts of medicinal plants have significant corrosion retardation in an acidic medium due to the fused ring and active groups of phytochemicals.

Moreover, polyphenolic and carbonyl groups are present in the extracts, as reported by Federico Ferreres *et al.*[23] which would lead to adhesion onto the mild steel surface, which acts as a barrier film in the corrosion medium.

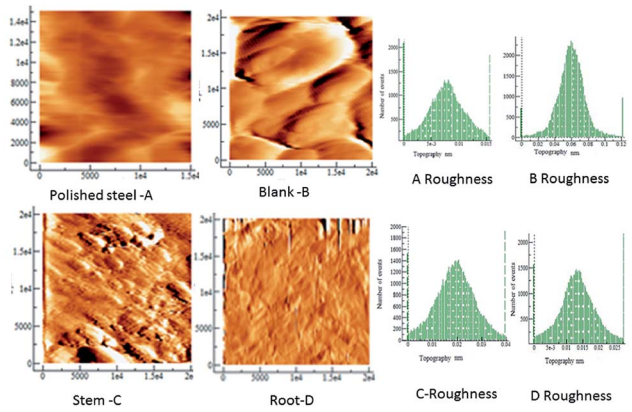

Fig. 6 AFM topographic of the mild steel coupons in the different exposure conditions to the *C. roseus* extracts, as indicated, polished steel, blank (left) stem (middle) root (right).

3.4. Microstructure analysis

Fig. 7 exhibits the results of FESEM after 5 days of immersing mild steel with and without inhibitor in NaCl (3.5%) medium. From the blank of this figure, it could be noted that without inhibitor the grain boundary of mild steel has severely damaged due to the attack of chloride ions on the surface.[42–45] Further, the results of elemental mapping indicate a higher concentration of oxygen due to the formation of oxide layers as well as the diffusion of dissolved oxygen on the steel surface. As shown in Fig. 7, due to the presence of inhibitor (root extraction), the roughness of mild steel decreased as compared to the absence of inhibitor and also localized corrosion does not appear due to the chemisorption of phytochemicals on the steel surface.

The elemental mapping suggested a decrease in the concentration of oxygen ions as compared to the blank, indicating an improvement in the corrosion inhibition efficiency of root's biofilm. As shown in Fig. 7(B), which is for the mild steel immersed in the extract of root, the roughness reduced to 140 nm as compared to the roughness of blank mild steel, which may be due to the covering of high surface area by the root phytochemicals and adsorbed on mild steel. As shown in Fig. 7, the morphology of mild steel immersed in the stem extract showed less pits on the surface due to the adsorbed active biofilm on the surface of mild steel and controlled pitting corrosion. The elemental mapping results indicate that the concentration of oxygen is less as compared to the roots extract. These outcomes signify that the phytochemicals of stem have

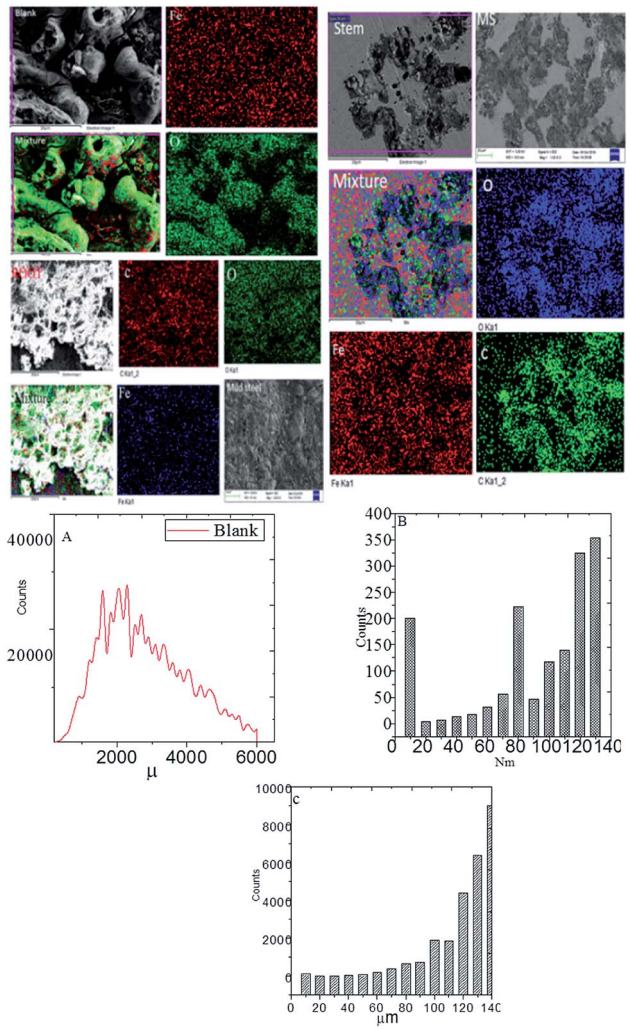

Fig. 7 Microstructure of mild steel immersed with and without inhibitor for 5 days in 3.5% NaCl medium mild steel roughness, and (A) blank mild steel roughness; (B) root mild steel roughness, and (C), stem mild steel roughness.

been chemisorbed by non-bonding electrons on the mild steel surface. Further, the polyhydroxyl groups of the phytochemicals of stem extract are chemisorbed on the mild steel surface. Hence, hydroxyl and carbonyl free electrons of stem extract are also assisting to the electrostatic attraction on the steel surface. As shown in Fig. 7(C), mild steel immersed in the phytochemicals of stem extract, it suggests that the roughness value has been reduced due to the adsorbed biofilm on the mild steel surface. The microscopy results suggest the *C. roseus* forms an excellent protective layer on the mild steel surface under salt environments.

Optical micrographs are exhibited in Fig. 8(A–D), where Fig. 8(A) (blank) is for mild steel without inhibitor, indicating the appearance of several pits on the mild steel surface due to the diffusion of chloride ions onto the grain boundary of mild steel. A study on different areas of steel surface for the diffusion of chloride ions shows the occurrence of uniform pitting corrosion (Fig. 8(B)). In Fig. 8(C) mild steel immersed in the

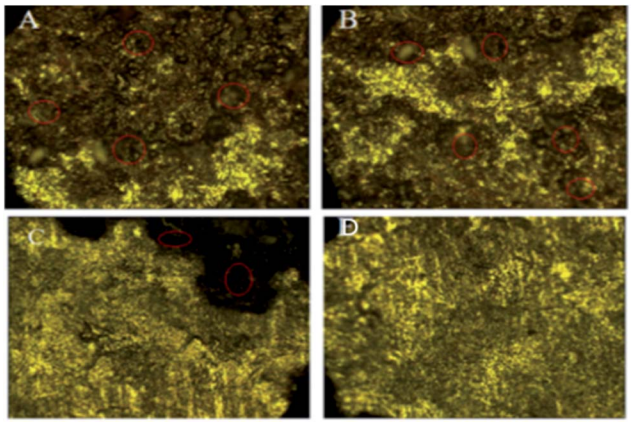

Fig. 8 Optical micrographs of mild steel after 5 days immersion in 3.5% NaCl medium with and without inhibitor molecules blank (A & B), root (C), and stem (D).

extract of root indicates localized corrosion retarded by the active phytochemicals adsorbed on the steel surface. Fig. 8 (D) is for the mild steel immersed in the extract of stem, showing a homogeneous MS surface and no propagation of pit corrosion on the steel surface due to strong chemisorption by the photochemicals of stem. The Raman spectra after corrosion treatment of mild steel immersed with and without inhibitor under NaCl (3.5%) environments are presented in Fig. 9. Before immersion, the peaks of native oxide layer of mild steel surface appear at 1230 cm^{-1} and the carbon peak of steel appears at 1600 cm^{-1}, confirming that the oxide layer is not formed on the surface.

Further blank surface peaks of MS appearing at 520 cm^{-1} and 680 cm^{-1} are due to magnetite and 730 cm^{-1}.[46–48] However, due to the presence of inhibitor molecules the oxide peak on mild steel decreased owing to the presence of biofilm. Further, the peaks appearing at 216 cm^{-1} and 290 cm^{-1} are attributed to the corrosion product of hematite on the mild steel surface. In the presence of inhibitor molecules, the intensity of the peaks of

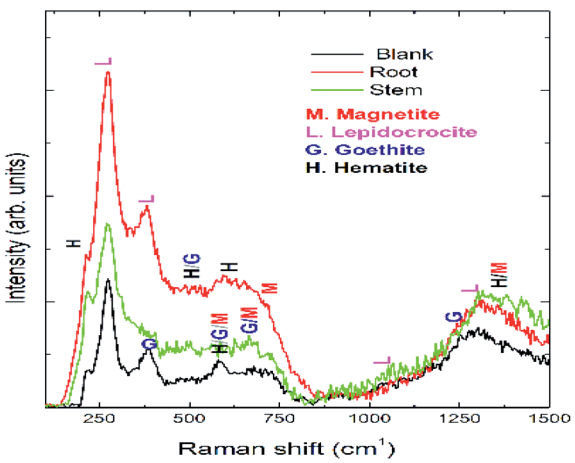

Fig. 9 Raman spectrum of mild steel after 5 days immersion in 3.5% NaCl solution with and without inhibitor molecules.

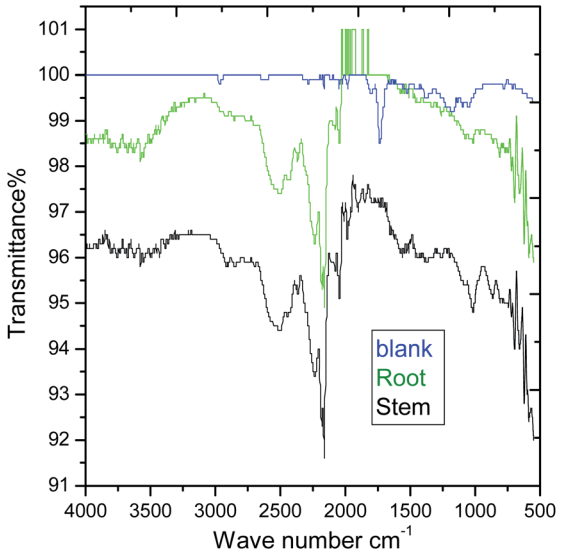

Fig. 10 AT-FTIR studies of mild steel surface after 5 days of immersion in 3.5% NaCl solution.

hematite, magnetite, and maghemite corrosion product decreased due to the presence of phytochemical complex film on the MS surface. Fig. 10 exhibits ATR-FTIR after the corrosion treatment of mild steel surface chemisorbed with phytochemicals. In the presence of root extract, the immersed mild steel surface shows a peak at 3500 cm^{-1} which is associated with the stretching of hydroxyl groups from the chemisorbed phytochemicals on the mild steel surface.

However, the C–H stretching frequency at 2800 cm^{-1} decreased as compared to before immersing with the extracted phytochemicals due to the physisorption on the mild steel surface. Further, the stretching frequency appearing at 2800 cm^{-1} is due to the adsorbed C–H groups on the surface.

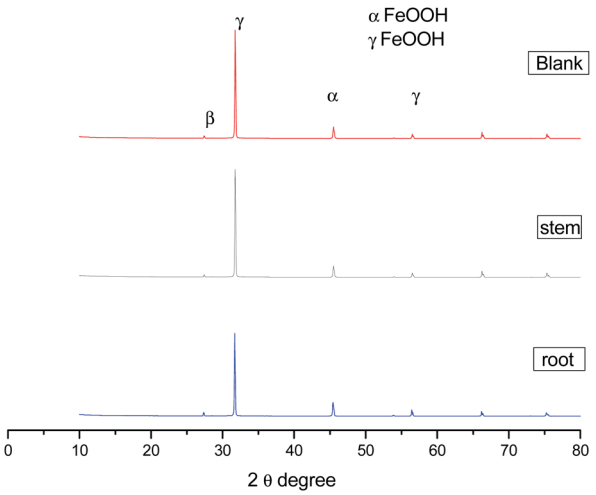

Fig. 11 XRD data of corrosion product on mild steel surface after 5 days immersion in 3.5% NaCl medium with and without inhibitor molecules.

The stretching frequency at 1600 cm^{-1} is associated with carbonyl group adsorbed on the mild steel surface.

Hence, the stretching frequency at 1000 cm^{-1} is related to the vibrations of C–O bond on the mild steel surface.[49–51] The spectroscopy studies confirmed the chemisorbed phytochemicals on the mild surface. As shown in XRD of Fig. 11, after 5 days of immersing mild steel in NaCl (3.5%) medium, the corrosion product of mild steel may be formed on the mild steel surface and the possible reactions are as follows.

$2Fe + 2H_2O$ ——— $2Fe(OH) + 2OH^- 2Fe(OH) + Cl^-$ (corrosion medium) Fe^+Cl^- (chemisorbed) $+ 2(OH)^- FeCl_2 + O_2$ (dissolved oxygen) $Fe^{2+} + Cl^- + FeOO^-$ (unstable)

$2FeOO^- + 2OH^- 2FeOOH$ (stable corrosion product) it may form Fe_2O_3/Fe_3O_4 on the mild steel surface.

The corrosion products have been confirmed by XRD. The peak appearing at $2\theta = 10$ °C is due to the formed iron oxide on the surface. Further, the peak appearing at around $2\theta = 40°$ suggesting the formation of magnetite (β-FeOOH) film on the mild steel surface.[52–55] The microscopy and spectroscopy studies suggest that the phytochemicals of *C. roseus* extract are physisorbed excellently on the mild steel surface.

3.5. Corrosion inhibition measurements

3.5.1. Weight loss. After 5 days of immersing mild steel coupons with and without the extract of *C. roseus* in NaCl solution (3.5%) are presented in Fig. 12. The presence of *C. roseus* extract (stem and root) on mild steel shows a greyish colour and there is no evidence of grain boundary and pit corrosion on the surface due to the adsorbed biofilm on mild steel surface. In the case of without inhibitor (blank), immersed in corrosion medium mild steel electrode localised corrosion is initiated on the surface as there is no biofilm in the blank solution, and chloride ion diffused into the MS surface. The corrosion inhibition efficiency of the extracts of *C. roseus* is related to the weight loss after immersing in mild steel, which is presented in Table 1. It could be noted from Table 1 that the extracts have significantly inhibited the progress of corrosion, where the stem extract of *C. roseus* is 4 times more effective than

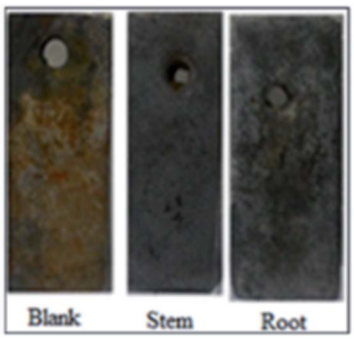

Fig. 12 The mild steel coupons after continuous immersion for 5 days in 3.5% NaCl solution and *C. roseus* extracts, blank (left) stem (middle) root (right).

the root extract,[56–58] which may be due to that the percentage of phytochemicals in the root is less as compared to stem. The observed difference in the corrosion inhibition efficiency might be due to the lower amount of active phytochemical constituents in root than stem.

3.5.2. Open circuit potential measurements (OCP). Before each electrochemical experiment, OCP measurements were carried out and the results are shown in Fig. 13. The OCP values of blank electrode decreased from −0.72 to −0.73 mV as mild steel undergoes corrosion. Correspondingly, the electrode immersed in the presence of root and stem extracts, the OCP value shifted from −72 to 0.68 mV as the phytochemicals of root and stem were adsorbed on the alloy surface. Finally, the OCP of the electrode immersed in the solution with the stem extract of *C. roseus* has a more positive value, −0.69 mV, suggesting that the phytochemicals of stem extract have a better electrode coverage as compared to the phytochemicals of root extract. Thus, the OCP values shifted toward positive value, indicating that the extracts of *C. roseus* function as a mixed type inhibitor.[59–61] Hence, the OCP results are supported with weight loss.

3.5.3. Potentiodynamic polarization. The polarization test was carried out to examine the impact of the corrosion inhibition of the extracts of *C. roseus* on mild steel in presence of NaCl (3.5%) environments[62] and the results are displayed in Fig. 14. Without *C. roseus* inhibitor molecules the corrosion current increased, and corrosion potential decreased because there is no barrier layer on mild steel surface. Whereas the diffusion of chloride ions on mild steel surface increased due to the absence of protective layer.[63] Hence, the cathodic hydrogen evolution of MS and anodic metal dissolution increased due to the mild steel grain boundary affected by corrosive chlorides ions diffusion rate increased as compared to presence of *C. roseus* extraction. However, the corrosion potential in the presence of inhibitor molecules of stem extract decreased due to the active *C. roseus* biomolecules bisindole chemisorbed on the active mild steel surface. Recently few green corrosion inhibiters in NaCl medium is reported. In case of ginger, *Persian liquorice*, and *Lemna gibba*, the active biochemicals[64–68] are polyphenolic active phytochemicals but in case of *C. roseus* the presence of bisindole moiety gives long time inhibition efficiency.

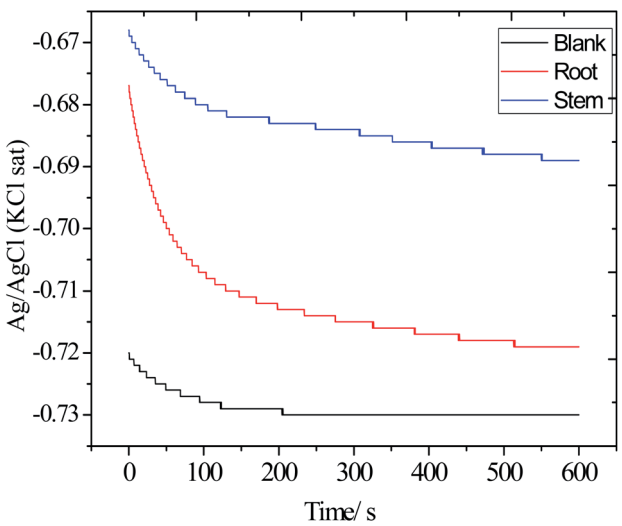

Fig. 13 The OCP values of the electrodes immersed in the 3.5% wt NaCl with and without inhibitor molecules.

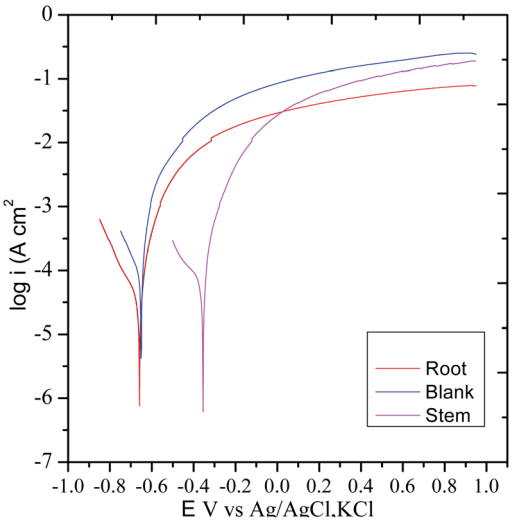

Fig. 14 Potentiodynamic polarization studies of *C. roseus* phytochemicals from different sources.

Hence, the presence of root extract corrosion current values decreased and the corrosion potential values increased due to the uniform protective film of active vindoline of *C. roseus* chemisorbed over the polarized steel surface. The corrosion inhibition efficiency values are presented in Table 2. The polyphenolics extracted from root and stem of *C. roseus* controlled the evolution of cathodic hydrogen and anodic metal dissolution due to the active bio molecules such as catharanthine adsorbed on the active mild steel surface.[69,70] On the other hand, the inhibition efficiency of root extraction decreased as compared to the phytochemicals of stem extract due to the presence of less active functional groups in the active biomolecules of root. Thus, the adsorption of *C. roseus* on mild steel has been confirmed through the surface studies of Raman, mapping, FESEM, ATR-FTIR, and XRD. The potentiodynamic polarization results are in agreement with the results of OCP.

3.5.4. Impedance studies. After 5 days immersion of mild steel in a corrosion medium, impedance studies were carried out and the obtained results are shown in Fig. 15(A–C). Without inhibitor molecules, for the case of immersed mild steel, the semicircle in Nyquist plot is suppressed due to the chlorides ion diffusion to the steel grain boundary.[71] Further, the mild steel charge transfer R_{ct} values decreased and C_{dl} double values increased due to the attack of chloride ions. Also, there is no protective film on mild steel surface, and therefore without inhibitor molecules mild steel undergoes corrosion. In addition, the impedance Bode plots and impedance frequency plots are suppressed due to the rate of chlorides ions diffusion increased to mild steel grain boundary.

Hence, in the presence of root extract immersed mild steel, the charge transfer R_{ct} values increased and double layer values

Table 2 Potentiodynamic polarization parameters for the *C. roseus* extracts

S. no.	$-E_{corr}$ (mV cm^{-2})	$-I_{corr}$ (mA cm^{-2})	η (%)	S.D	R_{ct} (Ω cm^{-2})	C_{dl} (μF)	η (%)
Blank	550	6.9			10	4.9716	
Root	650	2.5	63		500	2.2651	54
Stem	670	2.0	70	2.6962	880	1.2477	74

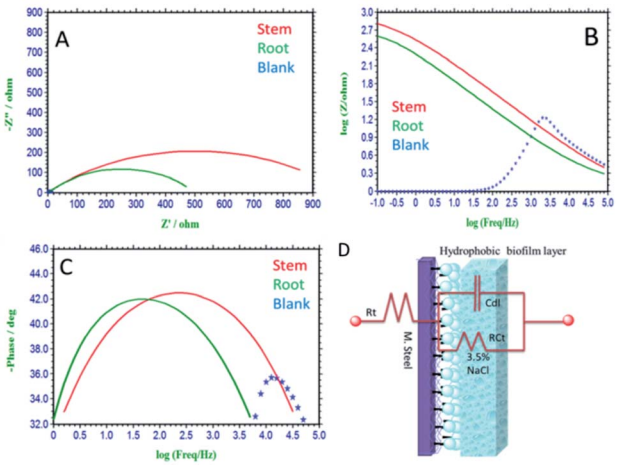

Fig. 15 Impedance studies of mild steel immersed for 5 days immersed in 3.5% NaCl medium with and without inhibitor molecules. (A) Nyquist plot, (B) frequency spectrum, (C) phase spectrum, (D) equivalent circuit proposed for the interface.

decreased due to the active biomolecules physisorbed on the alloy surface.

Further, the Bode phase plots and frequency plots show the increment of the adsorbed biofilm on the mild steel surface.[72] Whereas, in the presence of phytochemicals from the stem extract increased R_{ct} charge transfer values, due to the chemisorption of polyphenolic active biomolecules of secologanin on the mild steel surface. Further, the C_{dl} double value decreased as compared to blank due to the polyphenolic catharanthine coordinated to positively charged mild steel surface. The presence of active phytochemicals such as vindoline, catharanthine, is the key factor to improve the donation of electron to the metal surface.[73–76] As such the, catharanthine active nitrogen site acting as electron-donating groups could improve the passivation layer on mild steel surface. We believe that the secologanin polyphenolic species, are promoting the inhibition efficiency in 3.5% NaCl corrosion medium. The impedance values fitted with equivalents circuit are presented in Fig. 15(D), and the impedance values are listed in Table 2. The observed impedance values support the results from wettability studies of mild steel.

3.5.5. Quantum chemical study. The structure of major alkaloids present in *C. roseus*[23] are shown in Fig. 16. The HOMO and LUMO electron densities of the optimized structures of these alkaloids of *C. roseus* and two polyhydroxy fragments are shown in Fig. 17. The quantum chemical parameters are shown in Table 3. The electron densities corresponding to the π electrons of aromatic polyhydroxy and quinone fragments 3 and 4 are observed, suggesting the possibility of interaction between the empty iron d orbital of the metal atoms and π electrons of flavonoids.[77] The values of the highest occupied molecular orbital energy (ΔE_{HOMO}) and the lowest unoccupied molecular orbital energy (ΔE_{LUMO}) favour the adsorption of inhibitor molecules on the mild steel surface.[7] In general, HOMO energy is often related to the electron donating ability of inhibitor molecules, *i.e.* a high value indicates an increased tendency to donate a pair of electrons to the electron-deficient metal surfaces. On the other hand, a reduced LUMO value is associated to electron acceptance from higher energy level of metal d orbital.

The chemical softness (σ) and chemical hardness (η) values of the alkaloids of *C. roseus* favour to donate a pair of electron to the mild steel surface. Further, the electrophilicity (ω) and ΔN values favour for the inhibitor molecules to donate electron to vacant mild steel d orbital.[78] However, *C. roseus* flavonoids molecules HOMO–LUMO ΔE energy gap of main alkaloids 4.0196 eV, and fragments 4.0081 eV, ΔE 3.6292 eV values are close, as shown in Table 3. These values support the adsorption of phytochemicals on the mild steel surface. The adsorption of *C. roseus* is based on Lewis acid and base principle, where inhibitor molecules act as Lewis base and donate a pair of electrons to the d orbital of mild steel. Fig. 18 displays the results of the theoretical studies on the protonated active bio molecules of *C. roseus*.

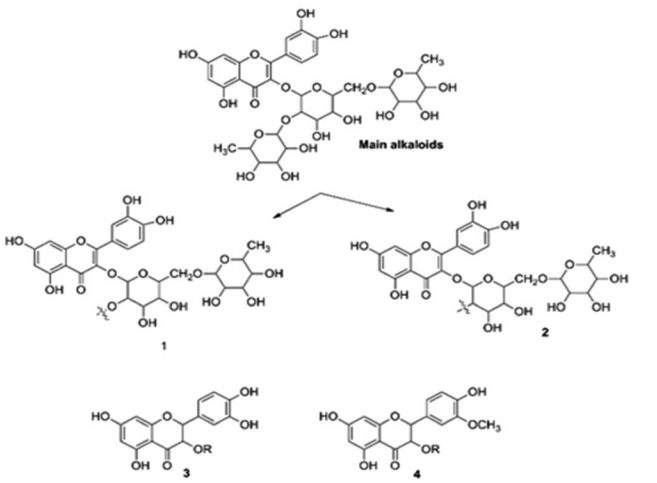

Fig. 16 Structures of the two main alkaloids, (1, 2) and two fragmentation residues (3, 4) of the *C. roseus* extracts.

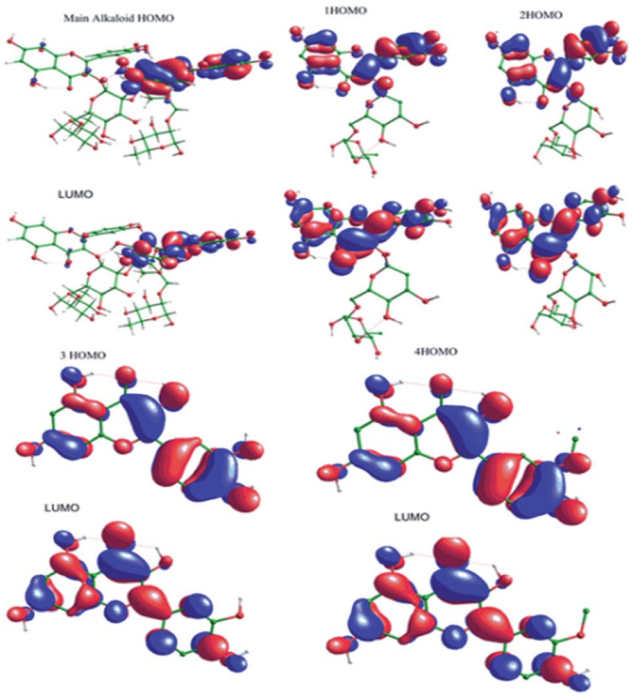

Fig. 17 HOMO and LUMO surfaces of neutral main alkaloids of *C. roseus*.

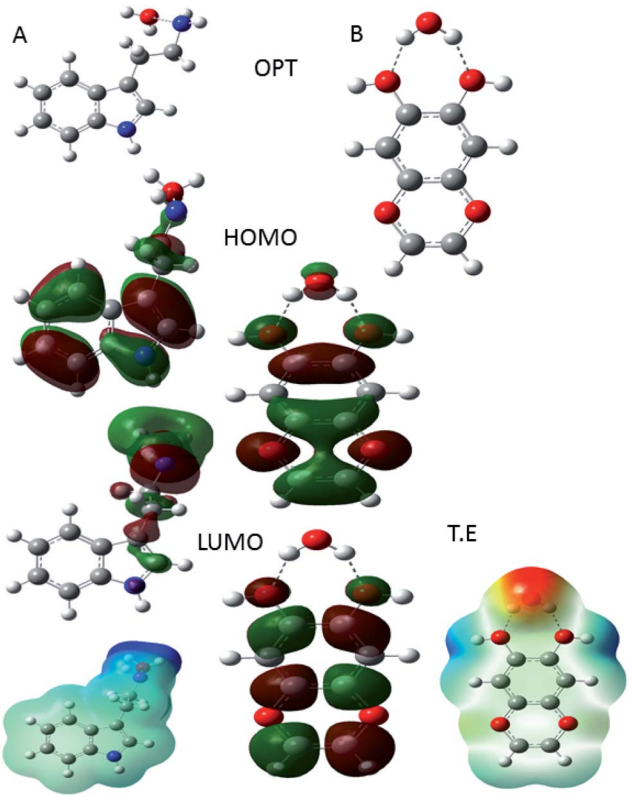

Fig. 18 DFT parameter of protonated indole (A) moiety and protonated active flavonoids of *C. roseus* (B).

In Fig. 18(A) HOMO and LUMO of indole moiety of *C. roseus* and (B) active flavonoid moiety is shown. In Fig. 18(A) indole moiety nitrogen and water molecules distance 1.5 Å and HOMO values is high it suggests that *C. roseus* bis indole active site improving the inhibition on mild steel in 3.5% NaCl environments. In addition, global softness values increased it another factor for *C. roseus* active biomolecules adsorbed on mild steel surface.[79] In another case flavonoid moiety suggest that hydrox groups interacted with water molecules and water molecules distance is 1.9 Å, HOMO energy associated with electron donating groups. Hence, the protonated flavonoid moiety LUMO energy has been decreased it indicates that *C. roseus* biomolecules strongly resistance corrosive ions interaction on mild steel surface.[80] The protonated form of active flavonoid biomolecules are leads to promote the inhibition efficiency long time.

3.5.6. Corrosion mechanism. As shown in Fig. 19. The corrosion inhibition mechanism of *C. roseus* indicates that polyphenolic fused rings and polyhydroxy carbonyl groups interact *via* non-bonding electrons on mild steel surface. Hence, the extract of *C. roseus* acts as a Lewis base and mild steel surface acts as a Lewis acid. Therefore, the inhibitor molecules are chemisorbed on the steel surface.[81–83] Although, the chemisorption of inhibitor molecules occurs through π electrons of phytochemicals and physisorption occurs *via* opposite charges of flavonoids to interact with mild steel surface. Whereas, the polyhydroxy groups of flavonoids interact with 111 surface irons. The HOMO energy is increased, whereas LOMO energy is decreased, which is associated with inhibitor molecules electrostatically interacting with the mild steel surface. Further, the frontier molecular orbital ΔE energy gap values are also close, which leads to the adsorption of inhibitor molecules on the mild steel surface. The phytochemicals of *C. roseus* act as a mixed type corrosion inhibitor in NaCl (3.5%) medium. The

Table 3 DFT computation results of *C. roseus* phytochemicals

S. no	HOMO (eV)	LUMO (eV)	$\Delta E_{\text{HOMO-LUMO}}$ (eV)	χ (eV)	η (eV)	σ (eV)	ω	Δ
1	6.2228	2.2146	4.0081	4.2187	2.0041	0.4990	4.4402	0.1544
2	6.2227	2.2741	3.9486	4.2484	1.9743	0.5065	4.5709	0.1533
3	5.9344	2.2087	3.6292	4.07155	1.8628	0.5368	4.4496	0.1652
4	5.8901	2.1475	3.5972	4.0188	1.8713	0.5343	4.3153	0.1680
M. Alkaloids	6.4034	2.3838	4.0196	4.3936	2.0098	0.4975	4.8023	0.1446
Indole-P	5.5962	1.2577	4.3385	3.4269	2.1692	0.4609	2.7068	0.6422
Flavonoid-P	5.2330	0.3752	4.8578	2.8041	2.4289	0.4117	1.6186	0.8299

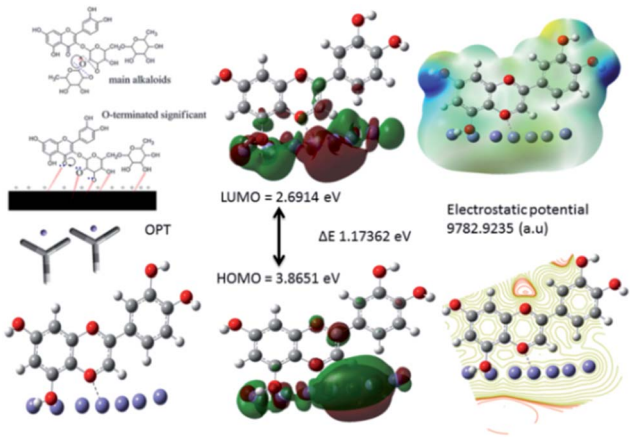

Fig. 19 Proposed scheme of *C. roseus* extracts adsorbed on 111 mild steel surface.

mixed type inhibitor could control the anodic and cathodic reaction on alloy surface. Spectroscopy and microscopy studies reveal that *C. roseus* is excellently adsorbed on the metal surface, and the obtained theoretical data well agree with the experimental results.

4. Conclusions

The extraction of the phytochemicals of *Catharanthus roseus* from its roots and stem have been accomplished by applying a fast ultrasonic energy method. The extracts were tested as corrosion inhibitors in mild steel surfaces using an aqueous NaCl (3.5%) medium. Spectroscopy studies indicate that the phytochemicals are adsorbed on the alloy surface. Further, the microscopy results indicate that the alkaloids of *C. roseus* are adsorbed on the mild steel surface, and the surface of mild steel is uniform as confirmed as compared with without *C. roseus* extraction. The studies of surface wettability suggest that polyphenolic active phytochemical constitutes are strongly chemisorbed. The electrochemical studies suggesting the retardation of anodic and cathodic progress reactions, *i.e. C. roseus* acts as a mixed type corrosion inhibitor in presence of salt environment. Quantum chemical study reveals that the extract of *C. roseus* is strongly adsorbed on the mild steel surface. The *C. roseus* showed inhibition efficiency 70% indicates that the *C. roseus* has excellent corrosion inhibition in 3.5% NaCl medium.

Conflicts of interest

There are no conflicts to declare.

Acknowledgements

NP thanks to Central University of Gujarat and Non-NET fellowship and Central Instrument Facility. The authors thank to Dr C. Balasubramanian at the Facilitation Centre for Industrial Plasma Technologies in the Institute for Plasma Research in Gandhinagar for AFM and to Mr Ravi Kumar at Indian Institute of Technology Bombay for quantum chemical study. FCB acknowledges SIP IPN 20194931 project for partial financial support.

References

1 F. Chen, Q. Zhang, J. Liu, H. Gu and L. Yang, *Ultrason. Sonochem.*, 2017, **37**, 267–278.
2 J. Deng, Z. Xu, C. Xiang, J. Liu, L. Zhou, T. Li, Z. Yang and C. Ding, *Ultrason. Sonochem.*, 2017, **37**, 328–334.
3 J. Liao, B. Qu, D. Liu and N. Zheng, *Ultrason. Sonochem.*, 2015, **27**, 1116.
4 H. L. Jiang, J. L. Yang and Y. Ping Shi, *Ultrason. Sonochem.*, 2017, **34**, 325–331.
5 T. Kidd, M. L. A. E. Easson, Y. Qu, G. Jones and V. De Luca, *Phytochemistry*, 2019, **159**, 119–126.
6 S. H. Moon, M. Pandurangan, D. H. Kim, J. Venkatesh, R. V. Patel and B. M. Mistry, *J. Ethnopharmacol.*, 2018, **217**, 107–117.
7 S. Both, F. Chemat and J. Strube, *Ultrason. Sonochem.*, 2014, 1030–1034.
8 W. Wang, Q. Li, Y. Liu and B. Chena, *Ultrason. Sonochem.*, 2015, **24**, 13–18.
9 M. B. Hossain, B. K. Tiwari, N. Gangopadhyay, C. P. O. Donnell, N. P. Brunton and D. K. Rai, *Ultrason. Sonochem.*, 2014, **21**, 1470–1476.
10 E. E. Oguzie, C. B. Adindu, C. K. Enenebeaku, C. E. Ogukwe, M. A. Chidiebere and K. L. Oguzie, *J. Phys. Chem. C*, 2012, **116**, 13603–13615.
11 E. E. Oguzie, K. L. Oguzie, C. O. Akalezi, I. O. Udeze, J. N. Ogbulie and V. O. Njoku, *ACS Sustainable Chem. Eng.*, 2013, **1**, 214–225.
12 D. I. Njoku, I. Ukaga, O. B. Ikenna, E. E. Oguzie, K. L. Oguzie and N. Ibisi, *J. Mol. Liq.*, 2016, **219**, 417–424.
13 H. Z. Alkhathlan, M. Khan, M. M. S. Abdullah, A. M. AlMayouf, A. Y. B. H. Ahmed, Z. A. AlOthmana and A. A. Mousa, *RSC Adv.*, 2015, **5**, 54283–54292.
14 C. Loganayagi, C. Kamal and M. G. Sethuraman, *ACS Sustainable Chem. Eng.*, 2014, **2**, 606–613.
15 H. Gerengi and H. I. Sahin, *Ind. Eng. Chem. Res.*, 2012, **51**, 780–787.
16 S. A. Umoren, Z. M. Gasem and I. B. Obot, *Ind. Eng. Chem. Res.*, 2013, **52**, 14855–14865.
17 A. Khadraoui, A. Khelifa, K. Hacham and R. Mehdaoui, *J. Mol. Liq.*, 2016, 293–297.
18 M. Prabakaran, S. Kim, V. Hemapriy, M. Gopiraman, I. S. Kim and I. M. Chung, *RSC Adv.*, 2016, **6**, 57144–57153.
19 F. Suedile, F. Robert, C. Roos and M. Lebrini, *Electrochim. Acta*, 2014, **133**, 631–638.
20 D. I. Njoku, Y. Lia, H. Lgaz and E. E. Oguziead, *J. Mol. Liq.*, 2018, **249**, 371–388.
21 D. I. Njoku, E. E. Oguzieb and Y. Li, *J. Mol. Liq.*, 2017, **273**, 247–256.
22 M. Ramezanzadeh, G. Bahlakeh, Z. Sanaei and B. Ramezanzadeh, *J. Mol. Liq.*, 2018, **272**, 120–136.
23 E. Arslan, A. A. Gürten, H. Z. Gok and M. Farsak, *ChemistrySelect*, 2017, **2**, 8256.

24 F. Ferreres, D. M. Pereira, P. Valentao, P. B. Andrade, R. Seab and M. Sotormayo, *J. Agric. Food Chem.*, 2008, **56**, 9967–9974.
25 E. E. Oguzie, D. I. Njoku, M. A. Chidebere, C. E. Ogukwe and G. N. Onuoha, *Ind. Eng. Chem. Res.*, 2014, **53**, 5886–5894.
26 A. Latnikova, D. Grigoriev, M. Schenderlein, H. Mohwald and D. Shchukin, *Soft Matter*, 2012, **8**, 10837–10844.
27 M. Bozorg, T. S. Farahani, J. Neshati, Z. Chaghazardi and G. M. Ziarani, *Ind. Eng. Chem. Res.*, 2014, **53**, 4295–4303.
28 P. M. Krishnegowda, V. T. Venkatesha, P. K. M. Krishnegowda and S. B. Shivayogiraju, *Ind. Eng. Chem. Res.*, 2013, **52**, 722–728.
29 U. M. Eduok, M. M. Khaled, A. B. Khalil, R. K. Suleiman and B. El Ali, *RSC Adv.*, 2016, **6**, 18246–18256.
30 C. Kamal and M. G. Sethuraman, *Ind. Eng. Chem. Res.*, 2012, **5**, 10399–10407.
31 D. Kumar Yadav and M. A. Quraishi, *Ind. Eng. Chem. Res.*, 2012, **51**, 8194–8210.
32 G. Ji, S. Kumar Shukla, P. Dwivedi, S. Sundaram and R. Prakash, *Ind. Eng. Chem. Res.*, 2011, **50**, 11954–11959.
33 M. Gopiraman, N. Selvakumaran, D. Kesavan, R. Karvembu and I. Soo Kim, *Ind. Eng. Chem. Res.*, 2012, **51**, 7910–7922.
34 D. Gopi, E. S. M. Sherif, V. Manivannan, D. Rajeswari, M. Surendiran and L. Kavitha, *Ind. Eng. Chem. Res.*, 2014, **53**, 4286–4294.
35 S. Ramesh and S. Rajeswari, *Electrochim. Acta*, 2004, **49**, 811–820.
36 E. E. Oguzie, Y. Lia and F. H. Wang, *Electrochim. Acta*, 2007, **52**, 6988–6996.
37 N. GoudIreni, R. Narayan, P. Basak and K. V. S. Raju, *New J. Chem.*, 2016, **40**, 8081–8092.
38 D. Gallant, M. Pezolet and S. Simard, *Electrochim. Acta*, 2007, **52**, 4927–4941.
39 I. Jevremovic, M. Singer, S. Nesic and V. M. Stankovic, *Corros. Sci.*, 2013, **77**, 265–272.
40 S. Nikpour, M. Ramezanzadeh, G. Bahlakeh, B. Ramezanzadeh and M. Mahdavian, *Constr. Build. Mater.*, 2019, **220**, 161–176.
41 N. K. Gupta, C. Verma, R. Salghi, H. Lgaz, A. K. Mukherjee and M. A. Quraish, *New J. Chem.*, 2017, **41**, 13114.
42 D. O. Grigoriev, K. Kohler, E. Skorb, D. G. Shchukin and H. Mohwald, *Soft Matter*, 2009, **5**, 1426–1432.
43 C. Verma, L. O. Olasunkanmi, I. B. Obot, E. E. Ebenso and M. A. Quraishi, *RSC Adv.*, 2016, **6**, 53933.
44 R. Haldhar, D. Prasad, A. Saxen and P. Singh, *Mater. Chem. Front.*, 2018, **2**, 1225–1237.
45 S. K. Saha and P. Banerjee, *Mater. Chem. Front.*, 2018, **2**, 1674.
46 Q. Li, Z. Feng, L. Liu, H. Xu, W. Ge, F. Lia and M. An, *RSC Adv.*, 2015, **5**, 32479.
47 N. Palaniappan, I. S. Cole, F. C. Briones, K. Balasubaramanian and C. Lal, *RSC Adv.*, 2018, **8**, 34275.
48 V. Ezhilselvi, H. Seenivasan, P. Bera and C. Anandan, *RSC Adv.*, 2014, **4**, 46293–46304.
49 I. S. Molchan, G. E. Thompson, P. Skeldon, R. Lindsay, J. Walton, E. Kouvelos, G. E. Romanos, P. Falaras, A. G. Kontos, M. Arfanis, E. Siranidi, L. F. Zubeir, M. C. Kroon, J. Klockner, B. Ilievd and T. J. S. Schubert, *RSC Adv.*, 2015, **5**, 35181–35194.
50 Q. Zeng, J. Zhang, H. Cheng, L. Chen and Z. Qi, *RSC Adv.*, 2017, **7**, 48526.
51 I. S. Molchan, G. E. Thompson, R. Lindsay, P. Skeldon, V. Likodimos, G. E. Romanos, P. Falaras, G. Adamova, B. Iliev and T. J. S. Schubert, *RSC Adv.*, 2014, **4**, 5300.
52 X. Wang, Y. l. Chen and G. Niu, *Corros. Eng., Sci. Technol.*, 2018, **53**, 54–64.
53 J. Haque, V. Srivastava, C. Verma, H. Lgaz, R. Salghi and M. A. Quraishi, *New J. Chem.*, 2017, **41**, 13647–13662.
54 A. L. Chong, J. I. Mardel, D. R. MacFarlane, M. Forsyth and A. E. Somers, *ACS Sustainable Chem. Eng.*, 2016, **4**, 1746–1755.
55 J. Yang, Y. Lu, Z. Guoa, J. Gu and C. Gu, *Corros. Sci.*, 2018, **130**, 64–75.
56 M. Prabakaran, S. H. Kim, V. Hemapriya, M. Gopiraman, I. Soo Kim and I. M. Chung, *RSC Adv.*, 2016, **6**, 57144.
57 R. M. Prest, G. Legay, S. Raveau, N. Chiffot and E. Finot, *Electrochim. Acta*, 2010, **55**, 2712–2720.
58 J. Wysocka, M. Cieslik, S. Krakowiak and J. Ryl, *Electrochim. Acta*, 2018, **289**, 175–192.
59 L. Bai, L.-J. Feng, H. Y. Wang, Y.-B. Lu, X.-W. Lei and F.-L. Bai, *RSC Adv.*, 2015, **54**, 716–4726.
60 X. Lei, H. Wang, Y. Feng, J. Zhang, X. Sun, S. Lai, Z. Wang and S. Kang, *RSC Adv.*, 2015, **5**, 99084–99094.
61 B. Xu, Y. Ji, X. Zhang, X. Jin and W. Y. Yizhong Chen, *RSC Adv.*, 2015, **5**, 56049–56059.
62 K. Zhang, B. Xu, W. Yang, X. Yin, Y. Liu and Y. Chen, *Corros. Sci.*, 2015, **90**, 284–295.
63 V. P. Singh, P. Singh, D. P. Singh, K. Tiwari, M. Mishraand and A. Singh, *RSC Adv.*, 2015, **5**, 45217–45230.
64 D. Yang, M. Zhang, J. Zheng and H. Castaneda, *RSC Adv.*, 2015, **5**, 95160–95170.
65 Y. Liu, Z. Song, W. Wang, L. Jiang, Y. Zhang, M. Guo, F. Song and N. Xu, *J. Cleaner Prod.*, 2014, **214**, 298–307.
66 E. Alibakhshi, M. Ramezanzadeh, S. A. Haddadi, G. Bahlakeh, B. Ramezanzadeh and M. Mahdavian, *J. Cleaner Prod.*, 2019, **10**, 660–672.
67 W. A. Mohamed, M. M. A. Mansour and M. Z. M. Salem, *J. Cleaner Prod.*, 2019, **10**, 846–855.
68 M. P. Casaletto, V. Figa, A. Privitera, M. Bruno, A. Napolitano and S. Piacente, *Corros. Sci.*, 2018, **136**, 91–105.
69 P. V. Hien, N. S. H. Vu, L. Xuan, N. Q. Tran, V. A. Dao, Q. T. Trinh and N. D. Nam, *New J. Chem.*, 2019, **43**, 15646–15658.
70 A. K. Singh and M. A. Quraishi, *Corros. Sci.*, 2011, **53**, 1288–1297.
71 D. d. l. Fuente, J. Alcantara, B. Chico, I. Diaz, J. A. Jimenez and M. Morcillo, *Corros. Sci.*, 2016, **110**, 253–264.
72 H. Gang, *Am. J. Appl. Chem.*, 2016, **4**, 207–211.
73 L. C. Murulana, M. M. Kaband and E. E. Ebenso, *RSC Adv.*, 2015, **5**, 28743.
74 H. Ishikawa, D. A. Colby and D. L. Boger, *J. Am. Chem. Soc.*, 2008, **130**, 420–421.
75 M. Magnotta, J. Murata, J. Chen and V. D. Luca, *Phytochemistry*, 2007, **68**, 1922–1931.

76 D. K. Liscombe and S. E. OConnor, *Phytochemistry*, 2011, **72**, 1969–1977.
77 V. Salim, B. Wiens, S. M. Atsumi, F. Yu and V. D. Luca, *Phytochemistry*, 2014, **10**, 23–31.
78 M. Breedon, M. C. Per, I. S. Cole and A. S. Barnard, *J. Mater. Chem. A*, 2014, **2**, 16660.
79 M. J. Frisch, G. W. Trucks, H. B. Schlegel, G. E. Scuseria, M. A. Robb, J. R. Cheeseman, G. Scalmani, V. Barone, G. A. Petersson, H. Nakatsuji, X. Li, M. Caricato, A. Marenich, J. Bloino, B. G. Janesko, R. Gomperts, B. Mennucci, H. P. Hratchian, J. V. Ortiz, A. F. Izmaylov, J. L. Sonnenberg, D. Williams-Young, F. Ding, F. Lipparini, F. Egidi, J. Goings, B. Peng, A. Petrone, T. Henderson, D. Ranasinghe, V. G. Zakrzewski, J. Gao, N. Rega, G. Zheng, W. Liang, M. Hada, M. Ehara, K. Toyota, R. Fukuda, J. Hasegawa, M. Ishida, T. Nakajima, Y. Honda, O. Kitao, H. Nakai, T. Vreven, K. Throssell, J. A. Montgomery Jr, J. E. Peralta, F. Ogliaro, M. Bearpark, J. J. Heyd, E. Brothers, K. N. Kudin, V. N. Staroverov, T. Keith, R. Kobayashi, J. Normand, K. Raghavachari, A. Rendell, J. C. Burant, S. S. Iyengar, J. Tomasi, M. Cossi, J. M. Millam, M. Klene, C. Adamo, R. Cammi, J. W. Ochterski, R. L. Martin, K. Morokuma, O. Farkas, J. B. Foresman, D. J. Fox, *Gaussian 09, Revision A.02*, Gaussian, Inc., Wallingford CT, 2009.
80 (*a*) C. Lee, W. Yang and R. G. Parr, *Phys. Rev. B: Condens. Matter Mater. Phys.*, 1988, **37**, 785–789; (*b*) P. J. Stephens, F. J. Devlin, C. F. Chabalowski and M. J. Frisch, *J. Phys. Chem.*, 1994, **98**, 11623–11627.
81 M. El Faydy, R. Touir, M. Ebn Touhami, A. Zarrouk, C. Jama, B. Lakhrissi, L. O. Olasunkanmi, E. E. Ebenso and F. Bentiss, *Phys. Chem. Chem. Phys.*, 2018, **20**, 20167–20187.
82 S. Mo, T. T. Qin, H. Q. Luo and N. Bing Lin, *RSC Adv.*, 2015, **5**, 9052.
83 N. Palaniappan, I. S. Cole, F. C. Briones, K. Balasubramanian and C. Lal, *RSC Adv.*, 2018, **8**, 34286.